

## 7A.2 **STORM STRUCTURE AND DECAY PROCESS OF THE 9 JUNE 2009 GREENSBURG, KANSAS SUPERCELL DURING VORTEX2**

Conrad L. Ziegler<sup>\*1</sup>, Michael I. Biggerstaff<sup>2</sup>, Louis J. Wicker<sup>1</sup>, Donald W. Burgess<sup>1,3</sup>, Edward R. Mansell<sup>1</sup>, Christopher M. Schwartz<sup>1,2</sup>, Paul Markowski<sup>4</sup>, Yvette P. Richardson<sup>4</sup>, and Christopher C. Weiss<sup>5</sup>

### 1. INTRODUCTION

Despite intensive study through remote sensing, in situ observations, and numerical modeling, both tornadogenesis and the development of the parent low-level mesocyclone in severe thunderstorms remains poorly understood. While results from the first Verification of the Origins of Rotation in Tornado Experiment (VORTEX, Rasmussen et al. 1994) in the mid-1990's produced new understanding of low-level rotation in storms, the influence of the local storm environment, and the importance of thermodynamic quantities in the rear-flank downdraft, the results also generated a new set of questions which illustrate that tornadogenesis is a complex process that involves a wide range of scales from the mesocyclone down to the flow next to ground in and near the vortex. It is not clear that one dominant tornadogenesis process in mesocyclonic supercells is responsible for the vortex formation; a variety of vertical vorticity sources (tilting of horizontal vorticity in the near-surface inflow (Wicker 1996), environmental heterogeneities (e.g., misovortices) along either pre-storm boundaries (Wakimoto et al. 1998) or in the vicinity of storm outflow boundaries (Wakimoto and Atkins 1996, Ziegler et al. 2001), or precipitation-induced downdrafts (Markowski et al. 2003) all seem to be viable candidates for tornado precursors.

Markowski et al (2002) and Grzych et al. (2007) employed mobile mesonet and radar observations to show that tornadogenesis likelihood increases with decreasing magnitude of the temperature deficit of the rear flank downdraft (RFD), indicating the importance of improving understanding of the origins and range of forcing of temperature and related

airflow perturbations in supercell RFDs to better anticipate tornadoes and their parent low-level mesocyclonic circulations. Examining the broader, storm-scale precipitation-filled boundary layer (BL), Doppler wind analysis (e.g., Brandes 1978) and modeling studies (e.g., Klemp and Rotunno 1983, Wicker and Wilhelmson 1995; Gilmore and Wicker 1998) have revealed a zone of intense convergence and baroclinicity on the storm-scale RFD's east flank of some supercells (i.e., "RFD boundary") that undercuts the classical forward flank downdraft (FFD) outflow, although this RFD boundary feature was not the focus of those earlier studies. (Here we distinguish the broad, "storm-scale RFD" from the connected but very localized, "occlusion RFD" within the low-level mesocyclone itself.) The storm-scale RFD is typically located within the classic supercell's precipitation core to the northwest of the developing low-level mesocyclone, as opposed to the classical RFD core centered to the southwest of the mesocyclone (Lemon and Doswell 1979).

A recent simulation study of the full 7-hour life cycle of the tornadic 22 May 1981 Binger, Oklahoma storm (Ziegler et al. 2010) reveals cyclic low-level mesocyclone intensifications following juxtaposition of the quasi-steady forward flank baroclinic zone with transient intensifications of the storm-scale RFD boundary and injection of a northerly flow of streamwise vorticity into the base of the main supercell updraft: this process triggers simulated occluding cyclic mesocyclogenesis (OCM) that is also broadly comparable to OCM simulated by Adlerman and Droegemeier (2005). Recent EnKF data assimilations of the 29 May 2004 Geary, Oklahoma tornadic supercell also reveal a (baroclinic) RFD boundary extending northward from the low-level mesocyclone (e.g., Ziegler et al. 2009). The classical solenoidal generation in the baroclinic forward-flank inflow region leads to initial low-level mesocyclone development (e.g., Klemp and Rotunno 1983, Rotunno and Klemp 1985), with intense stretching at the main updraft base dominating the mesoscale vortex intensification significantly above the surface due to vertical advection of vorticity (Wakimoto et al. 1998, Ziegler et al. 2001). The initial mesovortex would then act frontogenetically to intensify the storm-scale RFD boundary as in Doswell (1985). It appears likely that

*\*Corresponding author address:* Dr. Conrad L. Ziegler, National Severe Storms Laboratory (NSSL), 120 David L. Boren Blvd, Norman, OK 73072; email: [conrad.ziegler@noaa.gov](mailto:conrad.ziegler@noaa.gov)

<sup>1</sup>NOAA/NSSL, Norman, Oklahoma

<sup>2</sup>University of Oklahoma (OU), Norman, Oklahoma

<sup>3</sup>Cooperative Institute for Mesoscale Meteorological Studies/OU, Norman, Oklahoma

<sup>4</sup>The Pennsylvania State University, University Park, Pennsylvania

<sup>5</sup>Texas Tech University, Lubbock, Texas

the subsequent storm-scale RFD boundary may produce intensification of the near-ground mesocyclone by additional baroclinic generation of streamwise horizontal vorticity behind the shallow storm-scale RFD boundary followed by tilting/stretching.

Shabbott and Markowski (2006) showed that the temperature deficit of the forward flank downdraft (FFD) was positively correlated with sub-saturation or relative humidity (RH) of the inflow BL, with moister (drier) BLs associating with warmer (colder) downdrafts. Rotunno and Klemp (1985) used a cloud model to demonstrate that the air entering the wall cloud originates in the midlevel forward storm flank, with subsequent ingestion by the mesocyclone, development of the rainy FFD downdraft by loading and evaporation, and downward transport in descending easterly inflow to the updraft/wall cloud base. The key concept is that the saturation point (SP) level of the inflow air is lowered by evaporation, resulting in the characteristic lowered wall cloud base height relative to rain-free ambient updraft inflow air parcels. Gilmore and Wicker (1998) showed that modeled storm downdrafts are increasingly vigorous in environments with drier air from the elevated residual layer (hereafter, ERL) air. Descending, precipitation-free air would tend to warm and dry adiabatically, with diabatic moistening/cooling opposing RH decrease from downward displacement; thus the rainy downdraft character is likely a function of inflow SP, downdraft strength, and drop evaporation. In principle, given sufficient precipitation content the potential downdraft cooling could increase as the downdraft's proportion of ERL inflow increases relative to BL inflow. Details of mixing are not important to first order, as Betts (1984) showed that thunderstorm downdraft SP simply distributes along a moist virtual adiabat reflecting differing mixtures of BL and ERL downdraft air with concurrent diabatic cooling.

Convective storms often initiate in an environment possessing rather large values of convective available potential energy (CAPE) and low convective inhibition (CIN), and subsequently move into a stratified "inversion region" distinguished by cooler boundary layer (BL) temperatures and an elevated stable layer that may combine to suppress the storm (e.g., Doswell et al. 2002). Storms may experience variable lifetimes after entering inversion regions, presumably in relation to the magnitude of the stratification although for reasons that are not presently well understood. The demise of a majority of isolated, observed supercells analyzed by Bunkers et al. (2006) occurred either by weakening sufficiently to become non-supercellular or by decaying entirely. Graziano and Carlson (1987) showed that the likelihood of strong storms decreases with increasing

magnitude of the stratification of cool surface and BL temperatures beneath a warm, dry elevated residual layer (ERL) in "proximity" soundings containing high values of CIN and lid strength index (LSI). The 22 May 1981 Binger, Oklahoma supercell simulation study (Ziegler et al. 2010) demonstrated that the eventual storm decay involved a somewhat complex interaction between its cold pool, the cold ambient BL temperatures, the resultant movement of the FF baroclinic zone relative to the main updraft, and the strong inversion.

Investigation of the origins of downdrafts, their contribution to storm rotation through baroclinic and tilting/stretching effects, and the storm's interaction with a stable environment that promotes storm decay all require four-dimensional analyses of the storm's velocity, thermodynamic, humidity and hydrometeor fields. Ultimately, storm analyses that incorporate the full range of observational data from the VORTEX2 platforms (e.g., Doppler, polarimetric, in situ) could be input into an analysis that includes a full range of transportive and diabatic heating/cooling physics to determine downdraft origins and along-trajectory thermodynamics.

As an initial step to begin elucidating the origins of cold downdraft air and its role in the development of low-level rotation, the present study reports a preliminary storm-scale analysis of the late-mature and decaying stage of the 9 June 2009 Greensburg, Kansas supercell which was intensively observed during the VORTEX2 project. Multiple-Doppler radar analyses of time-varying 3-D airflow and reflectivity provide a context within which to interpret surface in-situ temperature and humidity measurements from mobile mesonets and StickNets in the storm and a mobile inflow sounding.

## 2. DATA SOURCES AND ANALYSIS METHODS

### a. VORTEX2 operations relative to storm evolution

Deep convection initiation occurred around 2200 on 9 June near a northeastward-advancing dryline-like boundary west of a stalled, decayed outflow boundary in the vicinity of Dodge City, Kansas. The initial storm initially moved east-northeastward, split and rapidly intensified just west of Dodge City around 2245, then crossed the weak cold front and subsequently turned slightly to the right as it moved over Dodge City around 2300. The initial deployment of the bulk of the VORTEX2 mobile assets engaged the storm beginning around 2315, and was followed by a redeployment of several mobile radars beginning around 2340 and continuing past 0030 until just prior to final storm decay. The latter radar deployment stage represents the focus of the present analysis.

Although the National Weather Service forecast office in Dodge City issued a tornado warning for the

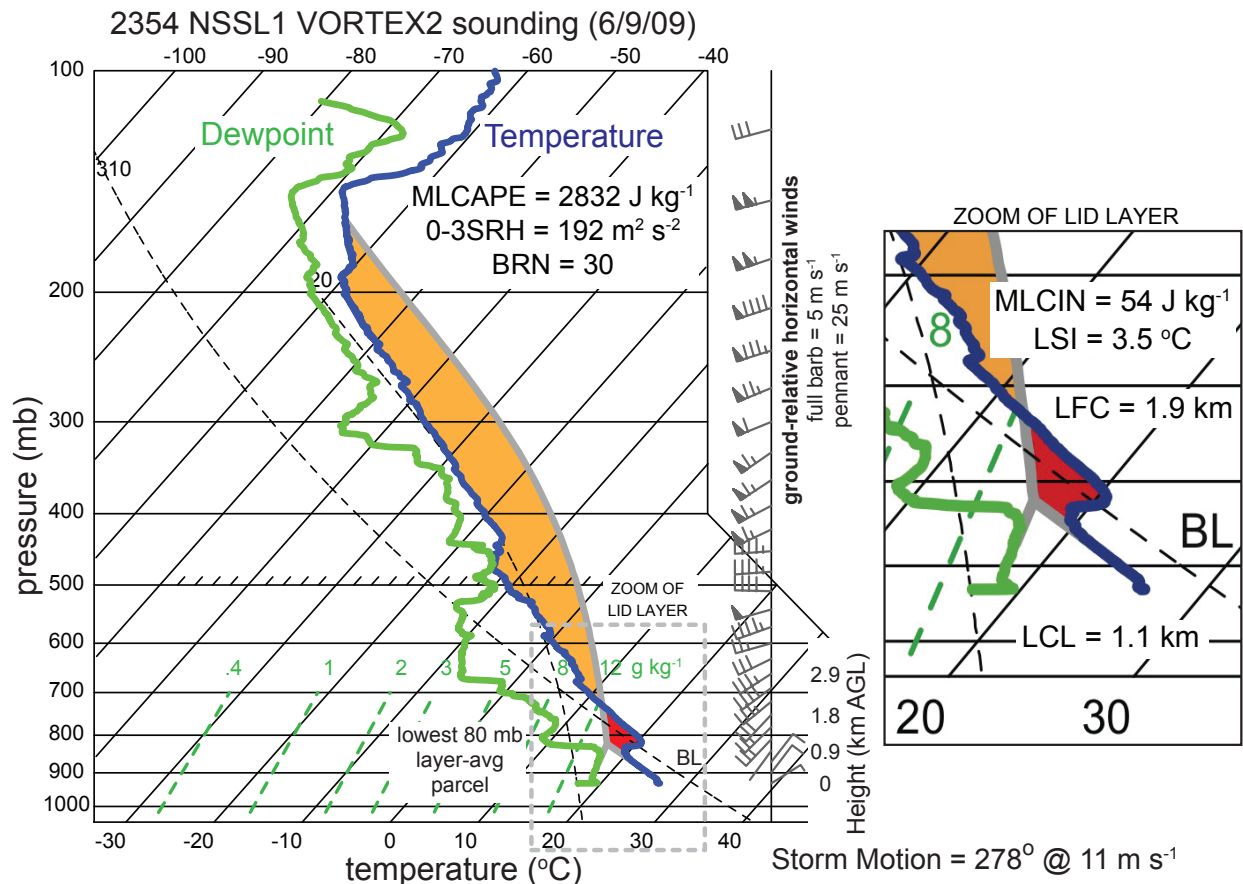


Figure 1: Skew-T, log-P plot of mobile sounding from NSSL1 launched 8 miles east of Greensburg, Kansas at 2354 UTC on 9 June 2009. Barbs display ground-relative winds, while 0-3SRH is computed from the observed (storm-scale analysis) updraft and mesocyclone motion from 278 degrees at 11 m s<sup>-1</sup>. MLCAPE (left panel) and MLCIN (right panel) are derived for the lifted parcel averaged over the lowest 80 mb. The maximum Parcel Theory updraft strength corresponding to the observed MLCAPE is about 75 m s<sup>-1</sup>.

Greensburg storm at 2340, the VORTEX2 teams did not visually identify a confirmed tornado. However, Storm Data lists the report of a small, short-lived tornado just after 2350 by non-VORTEX2-affiliated spotters. The DOW6 mobile X-band Doppler radar deployed in support of VORTEX2 detected intense, low-level gate-to-gate shears at 2340-2341 and again at 2348-2349, suggesting that two marginal tornadoes had occurred (Joshua Wurman, personal communication, 2009).

#### b. Multi-Doppler radar airflow synthesis

A multi-pass Barnes scheme (Majcen et al. 2008) is employed to spatially interpolate radial velocity and reflectivity observations from two or more Doppler radars to a 75 km x 75 km (horizontally) x 16 km deep analysis grid having a uniform grid spacing of 0.5 km. To obtain uniform smoothness of the storm-scale analysis over the *entire* storm-scale analysis domain while minimizing the amplitude of unresolved scales, the filtering parameter  $\kappa$  must be carefully chosen to obtain adequately strong damping

of scales less than  $\sim 3\Delta$  (where  $\Delta$  is the coarsest mean radar data spacing at any azimuth or elevation in the analyzed storm volume). The present (large-domain) storm-scale analysis requires a rather conservative choice of  $\Delta \approx 1.05$  km, which yields a Barnes filtering parameter  $\kappa = (1.33\Delta)^2 \approx 1.9$ . The analysis also assumes a Barnes convergence parameter value of  $\gamma = 0.3$ .

The 3-D vector airflow field is synthesized from the objectively analyzed multi-radar radial velocities using an “over-determined dual-Doppler” scheme based on iterative solution of two linear, normal equations for the u- and v-components with downward integration of the anelastic mass continuity equation to obtain the w-component (Ray et al. 1980, Kessinger et al. 1987). Combining data from three or more non-collinear radars effectively eliminates radar-baseline issues and (in a normal sense) improves the accuracy of the derived airflow.

A simple O’Brien-type column adjustment is applied to satisfy the assumed kinematic boundary condition ( $w = 0$ ) at the ground and local storm top.

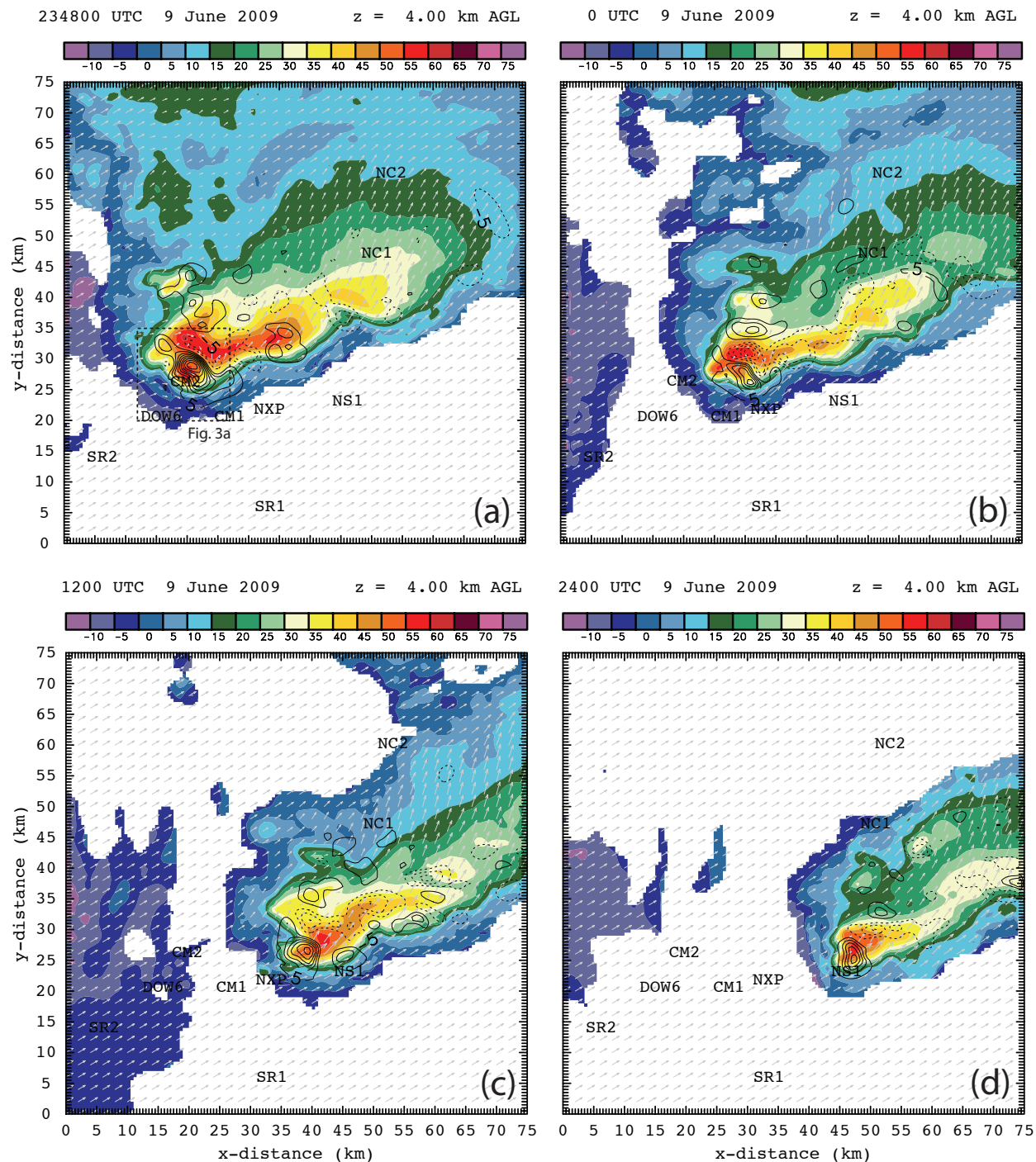


Figure 2: Time sequence of triple-Doppler radar analysis fields at 4.0 km AGL. (a) 2348 UTC on 9 June; (b) 0000 on 10 June; (c) 0012; (d) 0024. The entire (fixed, ground-relative) 75 km x 75 km analysis domain is shown. Radar fields include reflectivity (color-fill, dBZ), vertical velocity (contoured at 5 m s<sup>-1</sup> interval) and ground-relative horizontal wind vectors (scaled to 1 km = 15 m s<sup>-1</sup>). Symbols “SR1” and “SR2” locate the storm-scale radars, while KDDC is located at (-23.5, 40.3). Symbol “NS1” locates the 2354 NSSL1 environmental inflow sounding (Fig. 1). The dashed box locates the fine grid area shown in Fig. 3a.

An additional, inequality constraint adjustment prevents the w-component at any level from exceeding a fraction  $F_w$  (here,  $F_w \sim 0.8$ ) of the

maximum Parcel Theory updraft magnitude while maintaining regularity of the w-profile within each

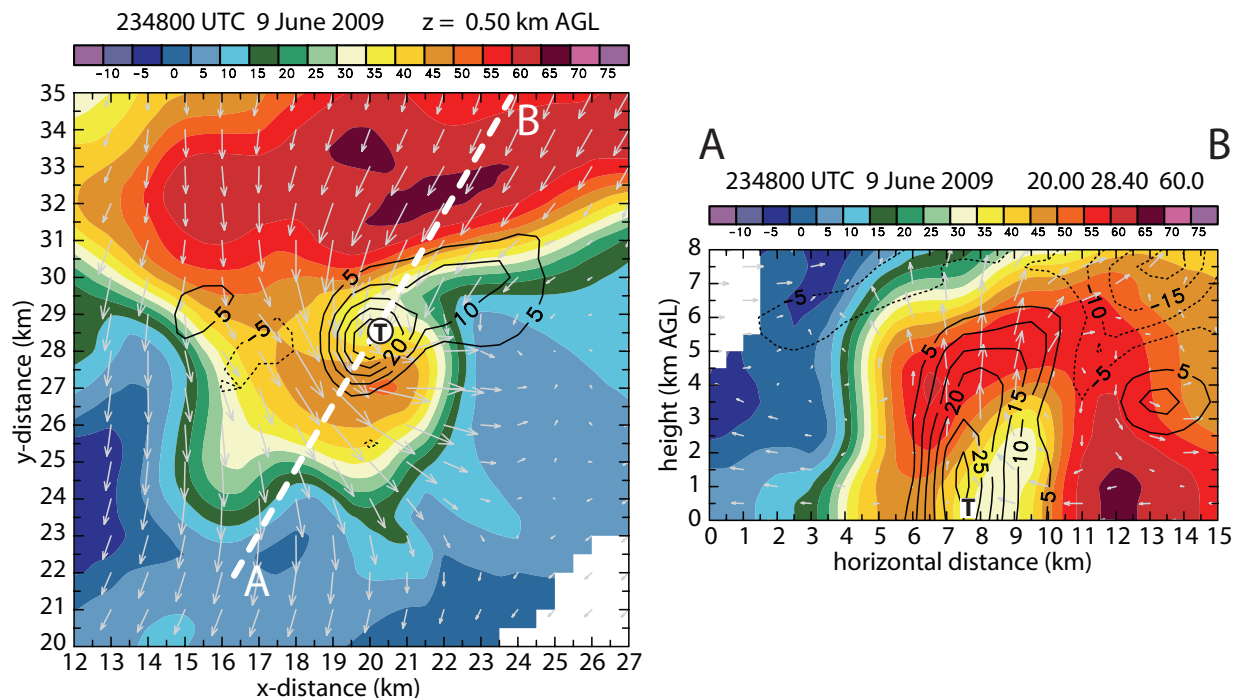


Figure 3: Triple-Doppler analysis of the storm’s core region at 2348. (a: left panel) Horizontal section of color-filled reflectivity (dBZ) with ground-relative horizontal wind vectors (scaled to 1 km = 15 m s<sup>-1</sup>) and contoured vertical vorticity (contour interval of 5 x 10<sup>-3</sup> s<sup>-1</sup> starting at +/- 5 x 10<sup>-3</sup> s<sup>-1</sup>); (b: right panel) as in (a), but within vertical cross-section A-B and ground-relative wind vectors in the A-B plane (scaled to 1 km = 40 m s<sup>-1</sup>). The approximate location of the DOW6-indicated marginal tornado at 2348-2349 (Joshua Wurman, personal communication, 2009) is indicated by the circled “T” and “T” in panels (a) and (b) respectively.

column (note, however, that the inequality constraint criterion was rarely incurred in this case).

The storm-scale Doppler radar observations were anchored by two mobile C-band SMART-radars (Biggerstaff et al. 2005). Due to the storm’s relative proximity to Dodge City, data from the WSR-88D radar KDDC also contributed to the storm-scale analysis. The effort to incorporate observations from the DOW6 and NOXP mobile X-band radars has begun (although results were not yet sufficiently matured to present at the conference.)

The storm-scale C-band radars typically collect data volumes in a different time sequence than the operational and mesocyclone-scale X-band radars (the latter being termed “non-synched” radars). To effect multi-radar wind synthesis, a technique known as “time-morphing” has been developed to produce synthetic time-synched analyses from the time-series of non-synched radar analyses. A two step method is followed: (1) shift the two neighboring non-synched analyses (gridpoint-by-gridpoint) either forward or backward in a time-to-space sense to the intermediate synthesis time using the storm motion and spatially interpolating the shifted, non-synched analysis values to the fixed synthesis grid; (2) time-weight the two non-synched, shifted analyses to produce the

synthetic analysis field value at each gridpoint. Spatial interpolation employs a trilinear polynomial to provide monotonicity. Viewing-angle distortion effects are negligible if the storm is removed from the radar site; and the time-weighting is distortionless for a synthesis time at the midpoint of the non-synched radar time interval.

#### c. In-situ storm observing platforms

Two sources of in-situ storm data are utilized in this study. Mobile mesonets are minivans equipped with rooftop weather stations that are driven both inside and in the near-environment of the storm (Straka et al. 1996). StickNets are tripod-mounted weather stations that are deployed along roads ahead of the storm and left in place as the storm moves across the sampling array (Weiss and Schroeder 2008). These in-situ data are post-processed to obtain values of in-situ potential temperature ( $\theta$ ), water vapor mixing ratio ( $q_v$ ), and virtual potential temperature ( $\theta_v$ ) using standard methods.

#### d. Storm environment

Mobile GPS-based sounding systems were deployed to obtain atmospheric profiles in the following regions in proximity to the Greensburg

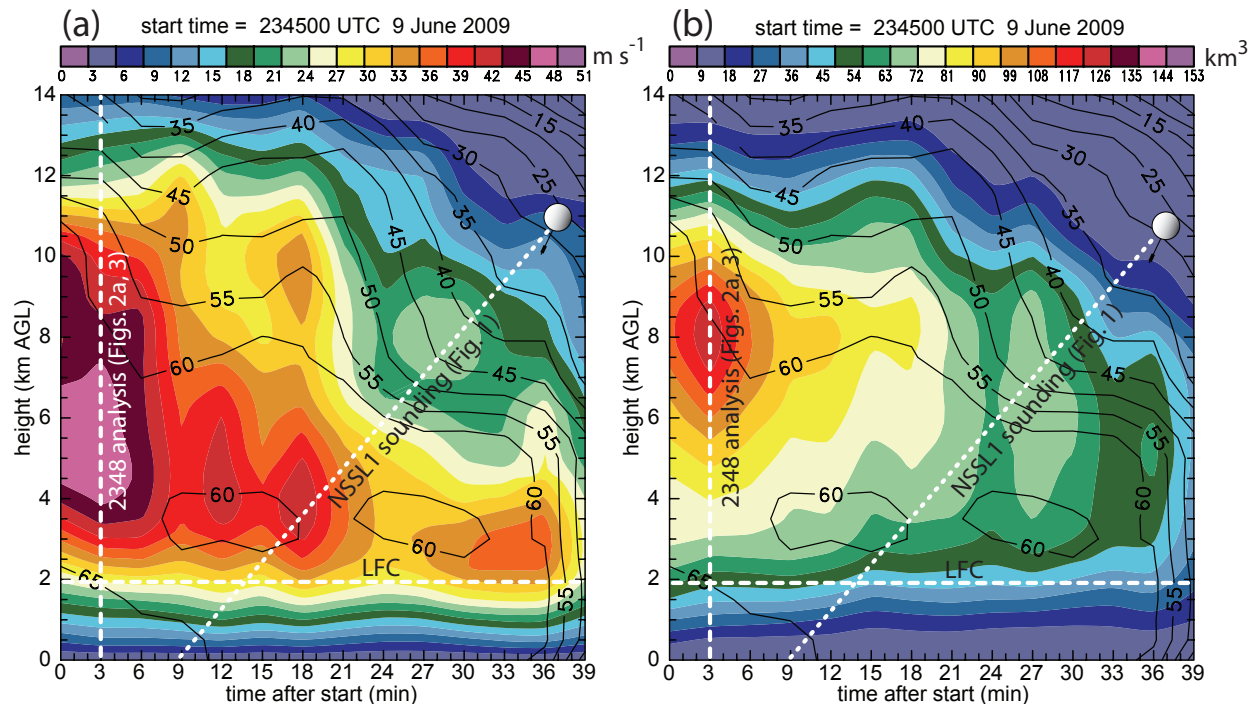


Figure 4: Time-height plots of (a) color-filled maximum updraft ( $m s^{-1}$ ) and (b) color-filled horizontally-integrated updraft volume  $> 5 m s^{-1}$  ( $km^3$ ) at each analysis level from 2345 to 0024. Reflectivity (dBZ) is contoured at an interval of 5 dBZ in both panels. The diagonal dashed lines denote the time-height ascent of the NSSL1 sounding, while the vertical dashed lines locate the time level corresponding to the 2348 wind analysis.

storm: (a) the low-level inflow at two times/locations during the storm's evolution; (b) the upstream environment; and (c) the leading edge of the forward-overhang stratiform precipitation beneath the storm's anvil cloud. For simplicity, the later inflow sounding obtained during the period of storm-scale radar analysis is emphasized in the present (preliminary) study.

The storm's inflow environment was sampled by the NSSL1 mobile sounding launched 8 miles east of Greensburg at 2354 UTC (Fig. 1). The sounding reveals sufficient potential instability for strong surface-based updrafts, given MLCAPE of over  $2800 J kg^{-1}$  (Fig. 1a). Although surface winds are rather weak and the low-level shear is approximately unidirectional, the rightward storm motion combined with the large vertical shear nevertheless associates with a 0-3SRH value exceeding  $190 m^2 s^{-2}$  that supports significant updraft rotation. However, the outflow BL is also quite stable given the sounding's convective inhibition (CIN) of over  $50 J kg^{-1}$  and lid strength index value of 3.5 (Fig. 1b).

### 3. DISCUSSION

#### a. Storm evolution from late-mature to decay stages (2345-0024)

The Greensburg storm initially had rather strong midlevel updrafts and high reflectivities, but

experienced a significant decline in intensity after  $\sim 2350$  (Fig. 2). The main updraft at 2348 (Fig. 2a) is centered at  $(x,y) = (20 km, 29 km)$  and has a peak value exceeding  $45 m s^{-1}$  (Fig. 3a). Due to the strong mid-tropospheric winds relative to the much slower eastward storm motion, the precipitation core advected far downstream. As the storm weakened, it increasingly acquired low-precipitation (LP) characteristics.

The supercellular character of the storm at 2348 during its late-mature stage was plainly evident in the juxtaposition of the intense storm-scale updraft with a strong low- and mid-level mesocyclone, a bounded weak-echo region, and a hook echo (Fig. 3). Furthermore, the approximate position of the DOW6-indicated marginal tornado at 2348 is rather consistent with the position and intensity of the low-level mesocyclone (Fig. 3a). A prominent wrapping rear-flank downdraft (RFD) outflow was in place to NW through SW of the low-level mesocyclone, and RFD outflow pushed far to the S and SW. A prominent FFD outflow was beginning to encroach on the low-level mesocyclone from the NE. The FFD was fed by strong downdrafts in the heavy-precipitation core to the NE of the low-level mesocyclone (Fig. 3b).

Though the storm was quite intense prior to 2350, it subsequently declined dramatically in overall intensity (Fig. 4). The overall depth of the dominant

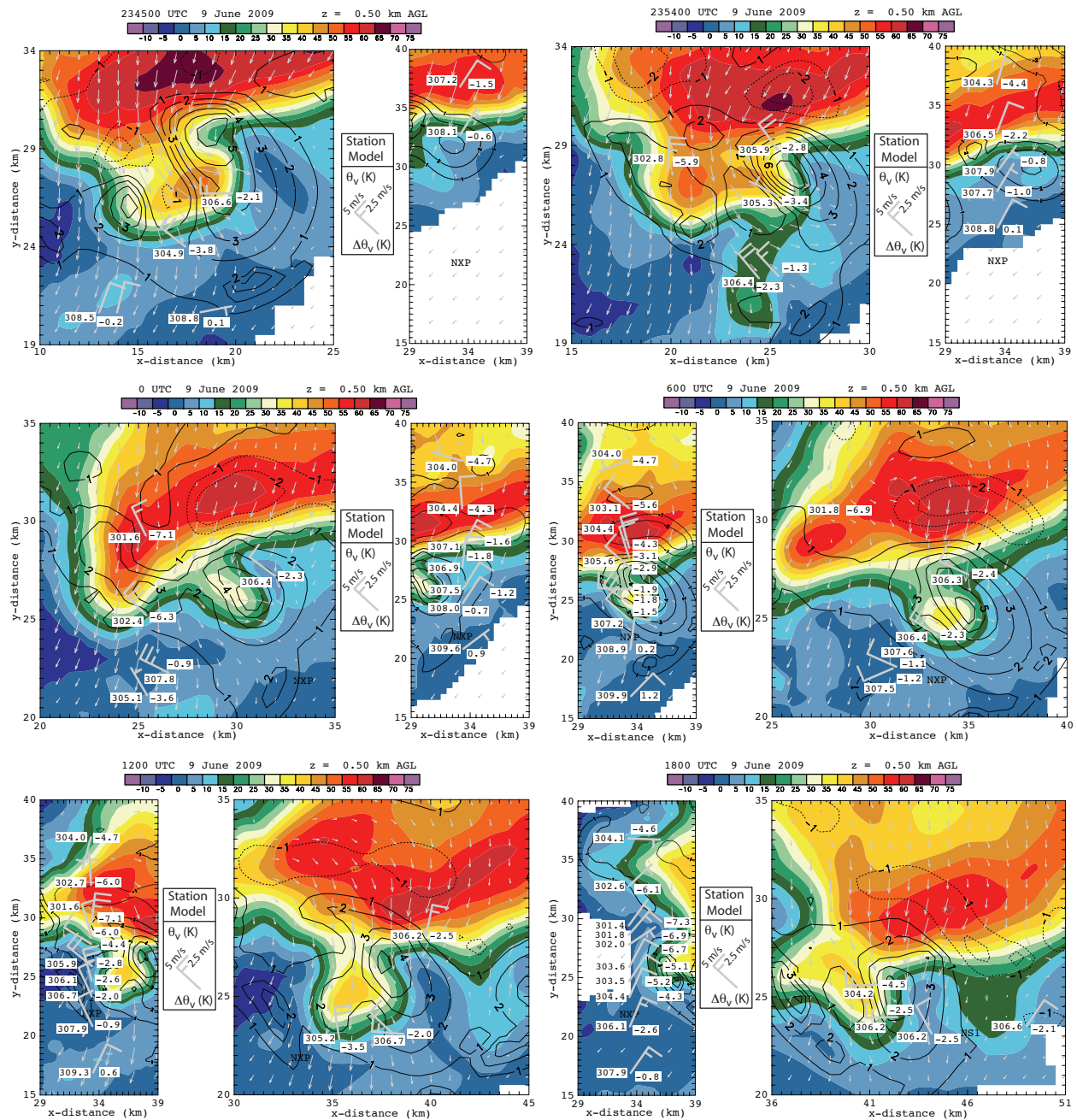


Figure 5: Time sequence of mobile mesonet (MM) and StickNet (SN) observations overlaid on radar analysis fields at 0.5 km AGL. (a: Upper left) 2345 UTC; (b: upper right) 2354; (c: center left) 0000; (d: center right) 0600; (e: lower left) 1200; (f: lower right) 1800. The station model includes the observed value of  $\theta_v$  and its deviation  $\Delta\theta_v = \theta_v - (\theta_v)_{env}$ , where  $(\theta_v)_{env}$  is the surface value obtained from the 2354 inflow sounding. The display area follows the storm motion: the 15 x 15 km and 10 x 25 km areas depict the MM and SN observations, respectively. Radar fields include reflectivity (color-fill, dBZ), vertical velocity ( $m s^{-1}$ ) and ground-relative horizontal wind vectors ( $1 km = 10 m s^{-1}$ ).

main updraft and precipitation core, the maximum updraft intensity, and the altitude of the maximum updraft all declined in phase (Fig. 4a). The level of the maximum updraft had a noticeable asymptotic behavior as it converged toward an altitude less than 1 km above the LFC from the 2354 NSSL1 inflow

sounding. As with peak updraft intensity, the volume of significant convective updrafts also declines with time (Fig. 4b).

These latter trends of storm intensity are collectively consistent with the hypotheses that (1) the mean MLCAPE of the inflow parcels was

decreasing rapidly with time and that (2) the storm's cold pool and forward-flank baroclinic zone were playing an increasing role with time to force the stable inflow air upward through the parcels' LFC. If hypothesis #1 were true, the actual *mean inflow parcel* LFC values should be trending upward somewhat with time. MLCAPE, MLCIN, and wind shear are all likely to be approximately constant over the rather short time scale of the observed decay process (i.e., ~ 30 min, equivalent to ~ 18 km of storm motion) given the observed cool, stably stratified inflow boundary layer conditions. Similarly, it is difficult to conceive how 0-3SRH and especially 0-6 km shear could decrease sufficiently within ~ 30 min to account for the observed storm decay (with or without any contribution from stabilizing inflow). If MLCAPE is approximately constant, the most probable explanation for a decreasing MLCAPE of the updraft inflow parcels would be a mean source level that rises above the moist boundary layer and taps increasingly warmer, drier air.

#### b. Cold pool and outflow evolution (2345-0024)

The interpretation of mobile mesonet and StickNet observations in the context provided by the storm-scale radar analysis permits inferences about how the cold pool evolves (if at all) and how its evolution correlates to the storm's overall weakening trend (Fig. 5).

At 2345, the StickNet array has just begun deploying on the southern edge of the FFD outflow while the mobile mesonets are primarily located within the storm-scale RFD outflow S of the low-level mesocyclone and are sampling  $\Delta\theta_v \sim -4$  °C (Fig. 5a). (A fifth mobile mesonet is probing the northern portion of the cold RFD precipitation core, which is outside the display domain of Fig. 5.) At 2354, the mobile mesonets are sampling  $\Delta\theta_v \sim -6$  °C in the southern RFD outflow and  $\Delta\theta_v \sim -3$  °C in the low-level mesocyclone immediately below the main updraft core (Fig. 5b). The StickNets are measuring  $\Delta\theta_v$  colder than  $-4$  °C in the FF precipitation core at 2354 (Fig. 5b). At 0000, the mobile mesonets are sampling  $\Delta\theta_v \sim -7$  °C in the RFD precipitation core while the StickNets are sampling  $\Delta\theta_v \sim -5$  °C in the FFD rain core (Fig. 5c). Also at 0000, the southernmost two mobile mesonets are sampling what appears to be the core and northern edge of a earlier, decayed pulse of cold-pool generated by the RFD at an earlier time.

From 0006 onward, the StickNets are sampling from the RFD precipitation core south through the RFD outflow to its trailing edge SW of the low-level mesocyclone (Fig. 5d-f). The backing trend of StickNet winds from 0000 to 0006 could imply that a forming low-level RFD outflow boundary extends

northward from the low-level mesocyclone to the RFD precipitation core. At 0006, the StickNets and mobile mesonets are sampling  $\Delta\theta_v \sim -5$  and  $-7$  °C, respectively, at different locations in the RFD precipitation core and are both sampling  $\Delta\theta_v \sim -2$  °C beneath the weakening main updraft (Fig. 5d). At 0012, the StickNets are sampling  $\Delta\theta_v$  as cold as  $\sim -7$  °C in the RFD precipitation core (Fig. 5e), a cold pool intensity almost identical to the measured mobile mesonet RFD cold pool intensity at 0000. At 0018, the StickNet is sampling  $\Delta\theta_v$  colder than  $-7$  °C in the precipitation-free RFD outflow W of the storm (Fig. 5f).

The evidence presented in Fig. 5 implies that the  $\theta_v$  deficits in the main RFD and FFD precipitation cores and their outflows are rather slowly changing (if at all) during the storm-scale observing period. On the other hand, there is limited evidence that the base of the main updraft may be experiencing cooling by the end of the analysis period due to encroachment of the expanding cold pool. Rather sparse samples of the FFD outflow south of the precipitation core imply that cold FFD outflow to the east of the wrapping RFD outflow is gradually progressing southward with time (Fig. 5a, b, c, f).

The in-situ wind measurements from the mobile mesonets and StickNets may be compared with the radar analyses to qualitatively estimate low-level wind shears (Fig. 5), at least to within the limits of local representativeness of the in-situ and radar measurements. The depth of the implied shear scales with the average altitude of the center of the main lobes of the storm-scale radars' base scan (~ 0.2-0.3 km). There is generally good agreement between surface in-situ and radar-analyzed winds at 0.5 km in the precipitation core and outflows, the notable exception being a consistently backed wind at the surface relative to 0.5 km to the west of the updraft and low-level mesocyclone (Fig. 5). Without independent in-situ storm-penetrating aircraft measurements to confirm the radar-analyzed winds, it may be difficult to quantify and explain these preliminary inferred wind shears on physical grounds.

The mobile mesonet and StickNet measurements may be subjectively combined to form a conceptual model of the Greensburg storm's low-level cold pool and ambient BL during its late-mature to decay stages (Fig. 6). The cold RFD is centered NW of the low-level mesocyclone, while less cold air extends eastward through the FFD core. A planned, more careful subsequent examination of the StickNet data may reveal the presence of secondary RFD and FFD boundaries north of the mesocyclone and on the southern edge of the precipitation core, respectively. One effect of the FFD moving south away from the precipitation core with time would be to progressively elevate the surface-based inflow

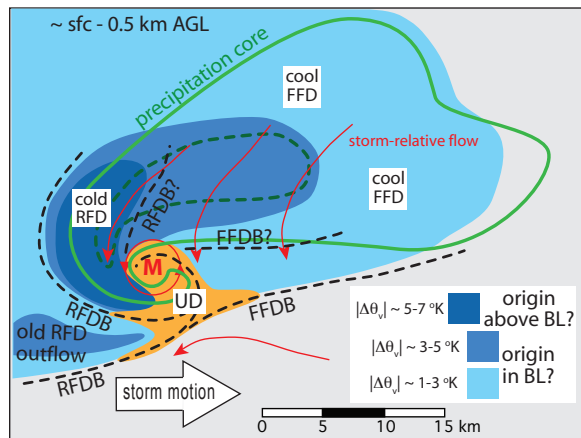


Figure 6: Conceptual model of the cold pool of the Greensburg storm during its late-mature to decay stages, based on integrated radar, mobile mesonet (MM), and StickNet (SN) observations. Orange-fill and symbol “UD” represent updraft, while “M” locates the low-level mesocyclone. Dashed black curves represent schematic locations of storm-induced surface boundaries (“FFDB” = forward-flank downdraft; “RFDB” = rear-flank downdraft). Cold pool strength is the difference of the ambient inflow theta-v at the surface from the 2354 sounding minus observed MM or SN values.

trajectories to the main updraft as the updraft base is displaced rearward toward the cold pool’s core. Indeed, it is conceivable that either the occurrence of marginal tornadoes or the premature termination of tornadogenesis in the Greensburg storm may have been due in part to the presence of cold outflow in the low-level mesocyclone (e.g., Markowski et al. 2002, Grzych et al. 2007).

#### 4. CONCLUSIONS

This preliminary analysis and integration of multiple Doppler radar, mobile mesonet, StickNet, and mobile sounding data suggests that the decaying updraft of the 9 June 2009 Greensburg, Kansas supercell storm was increasingly elevated as outflow spread southward beneath a strong post-frontal inversion. The  $\theta_v$  deficit in the low-level mesocyclone increased with time due to the intensification of the forward-flank downdraft outflow which converged with the wrapping rear-flank downdraft outflow, thus implying that the surface-based updraft may also have weakened by dynamically entraining northerly cold outflow. The storm’s RFD area had larger  $\theta_v$  deficits than its FFD, suggesting that potentially drier air may have descended from above the inversion. The comparison of the mobile mesonet and StickNet observations between 0000 and 1200 indicated that

the cold pool’s intensity was approximately constant with  $\Delta\theta_v \sim -7^\circ\text{C}$  during the storm’s decay stage.

Ongoing analysis of these data will include the calculation of air trajectories to test the hypothesis that cold (cool) downdrafts originate from the dry elevated residual layer and the moist boundary layer, respectively. An extension of a Lagrangian analysis technique that incorporates microphysical diabatic heating and cooling following the parcel motion could usefully augment the trajectory analysis by quantifying how downdraft source regions and radar-based storm microphysics assist the maintenance of the cold pool.

#### 5. ACKNOWLEDGEMENTS

Support for the present research was provided by the National Severe Storms Laboratory. Partial funding for this research was also provided by grants NSF-ATM-0802717, NSF-AGS-0801035, and NSF-AGS-0800542.

#### 6. REFERENCES

- Adlerman, E. J., and K. K. Droegemeier, 2005: The dependence of numerically simulated cyclic mesocyclogenesis upon environmental vertical wind shear. *Mon. Wea. Rev.*, 133, 3595–3623.
- Betts, A. K., 1984: Boundary layer thermodynamics of a High Plains severe storm. *Mon. Wea. Rev.*, 112, 2199–2211.
- Biggerstaff, M., L. Wicker, J. Guynes, C. Ziegler, J. Straka, E. Rasmussen, A. Doggett IV, L. Carey, J. Schroeder, C. Weiss, 2005: The shared mobile atmospheric research and teaching radar: A collaboration to enhance research and teaching. *Bull. Amer. Meteor. Soc.*, 86, 1263–1274, DOI: 10.1175/BAMS-86-9-1263.
- Brandes, E., 1978: Mesocyclone evolution and tornadogenesis: Some observations. *Mon. Wea. Rev.*, 106, 995–1011.
- Bunkers, M. R. Hjelmfelt, and P. L. Smith, 2006: An observational examination of long-lived supercells. Part I: Characteristics, evolution, and demise. *Wea. Forecasting*, 21, 673–688.
- Doswell, C. III, 1985: Reply. *J. Atmos. Sci.*, 42, 2076–2079.
- Doswell, C. A., III, D. V. Baker, and C. A. Liles, 2002: Recognition of negative mesoscale factors for severe-weather potential: A case study. *Wea. Forecasting*, 17, 937–954.

- Gilmore, M., and L. Wicker, 1998: The influence of midtropospheric dryness on supercell morphology and evolution. *Mon. Wea. Rev.*, 126, 943-958.
- Graziano, T. M., and T. N. Carlson, 1987: A statistical evaluation of lid strength index on deep convection. *Wea. Forecasting*, 2, 127-139.
- Grzych, M., B. Lee, and C. Finley, 2007: Thermodynamic analysis of supercell rearflank downdrafts from Project ANSWERS. *Mon. Wea. Rev.*, 135, 240-246.
- Kessinger, C. J., P. S. Ray, and C. E. Hane, 1987: The Oklahoma squall line of 19 May 1977. Part I: A multiple Doppler analysis of convective and stratiform structure. *J. Atmos. Sci.*, 19, 2840-2864.
- Klemp, J., and R. Rotunno, 1983: A study of the tornadic region within a supercell thunderstorm. *J. Atmos. Sci.*, 40, 359-377.
- Lemon, L. R., and C.A. Doswell, 1979: Severe thunderstorm evolution and mesocyclone structure as related to tornadogenesis. *Mon. Wea. Rev.*, 107, 1184-1197.
- Majcen, M., P. Markowski, and Y. Richardson, 2008: Multipass objective analysis of Doppler radar data. *J. Atmos. Oceanic Tech.*, 25, 1845-1858.
- Markowski, P., J. Straka, and E. Rasmussen, 2002: Direct surface thermodynamic observations within the rear-flank downdrafts of nontornadic and tornadic supercells. *Mon. Wea. Rev.*, 130, 1692-1721.
- Markowski, P. M., J. M. Straka, and E. N. Rasmussen, 2003: Tornadogenesis resulting from the transport of circulation by a downdraft: Idealized numerical simulations. *J. Atmos. Sci.*, 60, 795-823.
- Rasmussen, E.N., J.M. Straka, R. Davies-Jones, C.A. Doswell, F.H. Carr, M.D. Eilts, and D.R. MacGorman, 1994: Verification of the origins of rotation in tornadoes experiment: VORTEX. *Bull. Amer. Meteor. Soc.*, 75, 995-1006.
- Ray, P. S., C. L. Ziegler, W. Bumgarner, and R. J. Serafin, 1980: Single- and multiple-Doppler radar observations of tornadic storms. *Mon. Wea. Rev.*, 108, 1607-1625.
- Rotunno, R., and J. Klemp, 1985: On the rotation and propagation of simulated supercell thunderstorms. *J. Atmos. Sci.*, 42, 271-292.
- Shabbott, C., and Markowski, P., 2006: Surface in situ observations within the outflow of forward flank downdrafts of supercell storms. *Mon. Wea. Rev.*, 134, 1422-1441.
- Straka, J. M., E. N. Rasmussen, and S. E. Fredrickson, 1996: A mobile mesonet for finescale meteorological observations. *Journal of Atmos. and Oceanic Tech.*, 13, 921 - 936.
- Wakimoto, R. M., and N. T. Aktins, 1996: Observations of the origins of rotation: The Newcastle tornado during VORTEX 94. *Mon. Wea. Rev.*, 124, 384-407.
- Wakimoto, R.M., C. Liu, and H. Cai, 1998: The Garden City, Kansas, storm during VORTEX 95. Part I: Overview of the storm's life cycle and mesocyclogenesis. *Mon. Wea. Rev.*, 126, 372-392.
- Weiss, C. C., and J. L. Schroeder, 2008: The 2007 and 2008 MOBILE Experiment: Development and testing of the TTU StickNet platforms. Preprints, 24th Conference on Severe Local Storms, Savannah, GA, paper 5.1.
- Wicker, L. J., and R. B. Wilhelmson, 1995: Simulation and analysis of tornado development and decay within a three-dimensional supercell thunderstorm. *J. Atmos. Sci.*, 52, 2675-2703.
- Wicker, L. J., 1996: The role of near surface wind shear on low-level mesocyclone generation and tornadoes. Preprints, 18th Conf. on Severe Local Storms, San Francisco, CA, American Meteorological Society, 115-119.
- Ziegler, C. L., E. N. Rasmussen, T. R. Shepherd, A. I. Watson, and J. M. Straka, 2001: The evolution of low-level rotation in the 29 May 1994 Newcastle-Graham, Texas, storm complex during VORTEX. *Mon. Wea. Rev.*, 129, 1339-1369.
- Ziegler, C., L. Wicker, M. Biggerstaff, D. Betten, E. Mansell, K. Kuhlman, and D. MacGorman, 2009: Evolution of downdraft thermodynamics and low-level rotation in the tornadic 29 May 2004 Geary, OK, USA supercell storm. 5th European Conf. on Severe Storms, Landshut, Germany, pp. 29-30.
- Ziegler, C., E. Mansell, J. Straka, D. MacGorman, and D. Burgess, 2010: The impact of spatial variations of low-level stability on the life cycle of a simulated supercell storm. *Mon. Wea. Rev.*, 138, 1738-1766, doi: 10.1175/2009MWR3010.1.